Comparison of HH and VV Polarizations for Deformation Estimation using Persistent Scatterer Interferometry

Divya Sekhar Vaka[1], Shweta Sharma[2], Y.S.Rao[1]
[1]Centre of Studies in Resources Engineering, IIT Bombay, Powai-400076, Mumbai, India.
Email: sekharv@iitb.ac.in, ysrao@csre.iitb.ac.in
[2]Space Application Centre, ISRO, Ahmedabad-380015, India.
Email: shweta@sac.isro.gov.in

KEY WORDS: Time series, RADARSAT-2, Quad polarization, Urban Deformation, Vijayawada

ABSTRACT

Persistent Scatterer Interferometry technique (PSI) exploits time series of interferometric SAR data to estimate deformation over an area. The process involves analysing stable phase pixels from differential interferograms formed with respect to a single master. In this study, eight RADARSAT-2 C-band fine quad polarization images from 2014 to 2016 are used to identify Persistent Scatterer (PS) points and estimate deformation over Vijayawada city in India. With a full graph approach, 29 interferograms are generated. All the interferograms are unwrapped to aid stable deformation estimation. The prime objective of our research is to study the effect of HH and VV polarizations in PS point selection and deformation estimation. Initially, pixels with Amplitude Stability Index > 0.75 are selected as PS points. Later, PS pixels exhibiting temporal coherence > 0.75 and reflectivity > 1 are selected for deformation estimation. Before refinement, PS points for HH and VV polarization are identified as 49409 and 48395 respectively, whereas after refinement, they are about 24063 and 34389. Atmospheric Phase Screen (APS) is estimated and removed using a filtering approach. After APS removal, mean line of sight (LOS) displacement and velocity maps are generated. A linear model is used to invert displacements into velocities. Velocity obtained using HH polarized data ranges from +16 to -14 mm/year, and for VV it ranges from +12 to -19 mm/year. The deformation trend is linear throughout the observation period except in October 2014. Deformation around this month shows up and down pattern. We attribute this observation to the devastating Hudhud cyclone that hit the state of Andhra Pradesh in October 2014. Atmospheric variations due to the presence of strong troposphere component varied radar signal delay before and after the cyclone. Excluding this phenomenon, time series plots of selected points showed linear deformation pattern in both polarizations.

1. INTRODUCTION

Measuring magnitude and direction of displacement is the prime objective of any deformation estimation studies. Synthetic Aperture Radar Interferometry (InSAR) proved to be a prominent tool in precise mapping and measuring ground displacements with millimetre level accuracy. Differential SAR Interferometry (DInSAR) is widely used and applied to monitor land subsidence(Amelung et al., 1999; Massonnet et al., 1997), seismic deformations (Massonnet et al., 1993; Peltzer and Rosen, 1995), volcanic eruptions (Massonnet et al., 1995), landslides and glacier movements (Goldstein et al., 1993; Rao et al., 2004). However, limitations such as geometric decorrelation, temporal decorrelation, which cause incoherency and atmospheric variation between two satellite acquisitions, make conventional interferometry unsuitable for some studies (Hanssen, 2001). These DInSAR problems are addressed using multiple images over time. Time series analysis of InSAR data proved to be successful in mitigating atmospheric phase delays and other errors.

The concept of Permanent Scatterer Interferometry (PSInSAR™) was proposed (Ferretti et al., 2001, 2000) addressing DInSAR drawbacks. The technique addresses the problem by identifying scatterers called Permanent/Persistent Scatterers (PS), which are coherent over long time intervals. It is commonly referred as Persistent Scatterer Interferometry (PSI). PS are stable points on the ground surface like buildings, pipelines, electric poles, monuments or artificially installed corner reflectors (CR). Radar return from PS vary very little between acquisitions and the interferometric phase from these points is analysed to estimate deformation. PSI methods mainly vary in PS point identification and deformation estimation. Over the last two decades, several PSI methods were proposed based on temporal models (Colesanti et al., 2003; Ferretti et al., 2001; Kampes, 2006; Werner et al., 2003) and spatial correlation between pixels (Hooper et al., 2004). Another class of methods known as Small Baseline Subset (SBAS) were also proposed. SBAS methods use available pixels in all scene combinations, where the interferometric baseline is less than the critical baseline (Berardino et al., 2002; Lanari et al., 2004; Schmidt and Bürgmann, 2003). SBAS methods take benefit of expanded usable pixels for deformation estimation. A hybrid approach utilising both PSI and SBAS methodologies was proposed by Hooper (2008). The precision of velocity estimates using all these approaches ranges from 0.1 to 1 mm/year. Urban environments show high PS density, whereas rural areas show less number of PS due to the presence of agricultural fields, vegetated areas that vary with time (Hooper et al., 2004). On the other hand, areas affected by layover, foreshortening and shadow show less number of PS (Antonielli et al., 2016). Several studies were reported on monitoring urban subsidence using PSI and SBAS

methods. Most of them used single or multiple sensor datasets using HH polarization (Ng et al., 2012a; Wegmuller et al., 2010) or VV polarization (Ng et al., 2012b) images to study time series deformation over an area. Esmaeili and Motagh, (2015) applied optimised amplitude dispersion criteria to identify persistent scatterer candidates (PSC) and PS pixels in HH and VV polarizations. Using polarimetric data, they observed increment in number of PS pixels. In our study, we used both HH and VV polarizations of RADARSAT-2 C-band Quad polarization images. The prime objective of our research is to study the effect of HH and VV polarizations on PS point selection and deformation estimation over an urban area. SARPROZ, an SAR data processing tool written in MATLAB was used for data processing. It can handle high computational burdens and easily process a number of SAR images on multiple CPUs or computer clusters (Perissin et al., 2011).

2. STUDY AREA AND DATASETS

Vijayawada, a metropolitan city on the banks of Krishna River, located 30 km away from the recently announced Andhra Pradesh (AP) state capital is chosen as our study area. The city of Vijayawada, Machilipatnam comes under Andhra Pradesh Capital Region (APCR). Situated on the banks of Krishna River, covered by hills and canals, the jurisdiction of the city under Vijayawada Municipal Corporation is spread over an area of 61.8 sqkm. Prakasam barrage, a major dam constructed over River Krishna, is the main source of water for the region. Three canals originating from Prakasam reservoir flow through the city. Andhra Pradesh owes its rich agriculture practice to the Prakasam dam. The city has a tropical climate with annual mean temperatures ranging between 23–34ºC and annual mean rainfall around 98cm. It receives most of its rainfall from Southwest and Northeast monsoons. The city witnessed rapid growth in urban infrastructure due to its proximity to the new AP state capital Amaravati.

In our study, we processed and analysed time series spaceborne satellite data to understand the ground surface deformation pattern. We used eight ascending pass images of RADARSAT-2 Quad polarization C-band data to map deformation of Vijayawada between 2014 and 2016. We processed HH and VV polarization images to estimate deformation and also to study the effect of polarization on deformation estimates. Figure 1 shows footprints of RADARSAT-2 images over laid on Google Earth imagery. RADARSAT-2 is an Earth observation satellite launched on December 14, 2007 for the Canadian Space Agency (CSA) and operated by MacDonald Dettwiler and Associates (MDA).

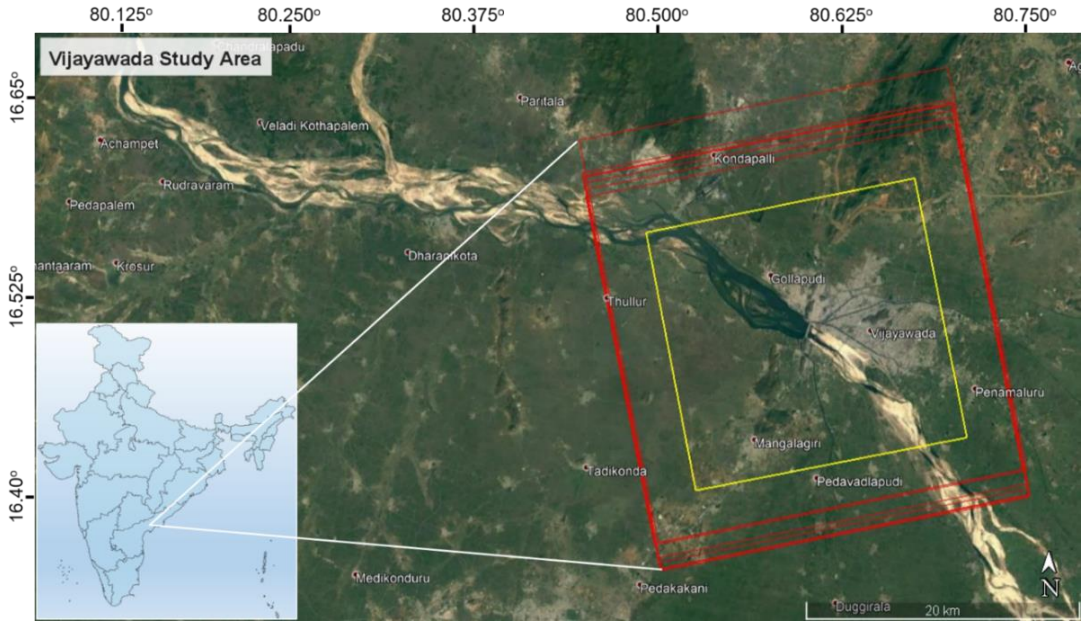

Figure 1: Footprints of RADARSAT-2 images (red polygons) overlaid on Google Earth imagery. Yellow polygon represents an area of interest (AOI) of this study. The inset shows the location of the study area in India map. RADARSAT-2 Data and Products © MacDonald, Dettwiler and Associates Ltd. 2014 – All Rights Reserved. RADARSAT is an official trademark of the Canadian Space Agency.

Table 1 shows the list of data and corresponding parameters used for this study. We calculated perpendicular baseline ($B_{\perp}$), temporal baseline (B_T) and height ambiguities (h_A) with respect to the master image (10-12-2014). Though Table 1 showed the values with respect to a single image, we did not use single master approach to estimate deformation. We used full graph approach that generated 29 interferograms with perpendicular baselines less than 250m. This enabled us to increase data density even though only eight images are available. The increase in data density will improve deformation estimation stability. Figure 2 shows images graph showing connections and perpendicular baselines between images.

Table 1: RADARSAT-2 data used for the study. Perpendicular baseline ($B_\perp$), temporal baseline (B_T) and height ambiguities (h_A) are calculated with respect to master image (10-12-2014).

S.No.	Date of acquisition	Incidence angle (degrees)	$B_\perp$(m)	B_T (days)	h_A (m)
1	08-01-2014	40.8	56.08	336	-16.31
2	29-09-2014	40.8	24.34	72	-1.60
3	23-10-2014	40.8	-77.20	48	57.42
4	16-11-2014	40.8	-100.35	24	28.02
5	10-12-2014	40.8	0	0	∞
6	27-05-2015	40.1	-51.78	-168	-48.46
7	03-04-2016	40.5	68.21	-480	-12.0
8	08-07-2016	40.5	-205.60	-576	-55.05

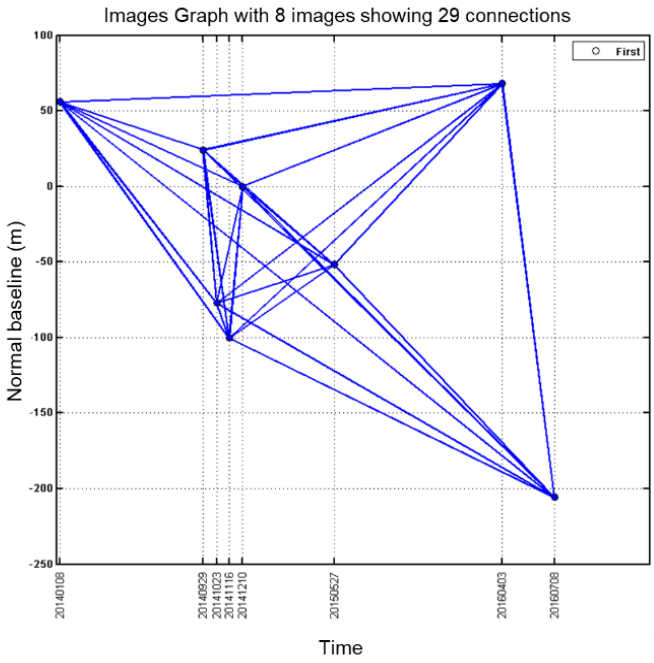

Figure 2: Images graph showing connections between satellite images. Twenty-nine connections between images are formed using eight RADARSAT-2 ascending pass images between 2014 and 2016.

3. METHODOLOGY

All images are coregistered and resampled with respect to a single master image, which is acquired on 10-12-2014. Using a full graph approach, 29 interferograms are generated with perpendicular baselines less than 250m. Topographic phase is removed using 1arcsec SRTM DEM. Using Minimum Cost Flow (MCF) approach, we unwrapped differential interferograms. Unwrapped interferograms are generated after topographic phase removal. These are given as input to time series analysis. Time series analysis is carried out for HH polarisation images as well as for VV polarization images. Followed methodology is presented as a flowchart in Figure 3.

Amplitude images are calculated from SLCs and PS points are selected based on an amplitude-based criterion. Initially, we chose Amplitude Stability Index (ASI) > 0.75 to select PS points. This criterion is equivalent to Amplitude Dispersion (D_A) < 0.25. The relation between ASI and D_A is given as:

$$ASI = 1 - D_A = 1 - \frac{\sigma_A}{\mu_A} \quad (1)$$

where, σ_A, μ_A are standard deviation and mean of amplitude respectively. Even though, high ASI value is chosen, there exists a good probability for PS point identification in urban areas. In addition, the number of images over the

study area are very less and sparsely distributed in time. Therefore, we have imposed strict criteria, which help in accurate deformation estimation selecting only stable PS points. We have adopted a linear model for deformation estimation. Further, PS points with low coherence are filtered by imposing a threshold on temporal coherence (> 0.75). A reflectivity map is calculated by temporal averaging of SAR amplitude images. Reflectivity is a measure of amplitude in volts, which is in our case normalised between 1 and 3. In logarithmic scale, reflectivity is similar to backscattering coefficient(σ_o). We have also chosen reflectivity (> 1) as an additional criterion to mask out any PS points over water surfaces and incoherent areas. We have removed atmospheric phase delays by high-pass filtering in the time domain and low-pass filtering in the spatial domain. Estimated deformation phase of each PS pixel is converted into range change measurements. Velocity maps showing deformation per year for both HH and VV polarizations are generated. Deformation includes both subsidence and uplift phenomena. We have also analysed displacement by plotting temporal trend of selected points.

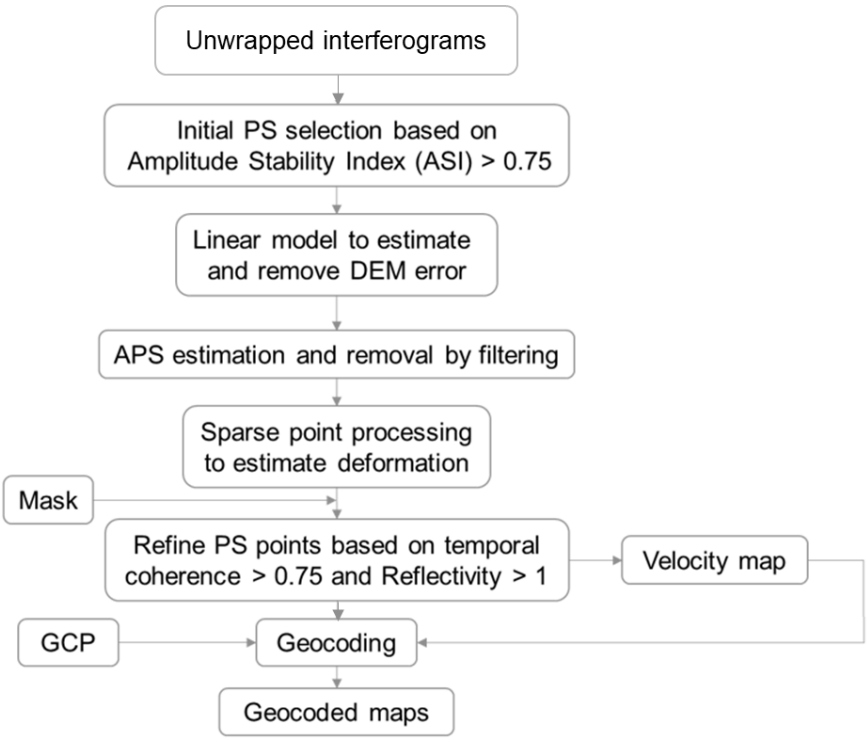

Figure 3: Methodology followed for deformation estimation over Vijayawada.

4. RESULTS AND DISCUSSION

Time series analysis of 29 unwrapped interferograms produced notable deformation. Table 2 shows the number of PS points identified with ASI > 0.75. We identified 1014 more PS points in HH compared to VV polarization. At a later stage, to identify more stable PS points, we imposed strict criteria on PS point selection to improve the stability of deformation results. At this stage, PS points with temporal coherence > 0.75 and reflectivity > 1 are chosen for deformation estimation. In both polarizations, refinement leads to severe decrement in the number of PS points. Due to refinement criteria, HH polarization is mostly affected. HH shows a reduction of 25346 PS points, whereas VV shows a reduction of 14006 PS points only. The number of PS points identified after refinement (VV>HH) is opposite to that of initial selection (HH>VV). Now, VV shows a high number of PS points than HH polarization. The response of VV polarization to urban environment is dominant than HH. The vertical orientation of urban buildings or settlements produce a double bounce, which result in high backscattering from the targets. This result in a strong and stable returns from the targets over time. Although initially, we have identified more PS points, refinement show that VV responds more to the vertically orientated structures than HH. Few non-urban areas are also identified in VV polarization compared to HH, which lead to increase in number of PS points. PS points are overlaid on reflectivity map. Figure 4 shows the number of PS points in both polarizations. Careful visualization and comparison of both velocity maps with Vijayawada study area shown in Figure 1, it is observed that major portion of urban built-up is identified as PS points in VV polarization as compared to HH. The range of deformation is also more in VV as compared to HH.

Table 2: Number of PS points identified during initial selection and refinement

Parameter	HH	VV	Difference between HH and VV PS points
ASI > 0.75	49409	48395	**1014**
Temporal Coherence > 0.75 & Reflectivity > 1	24063	34389	**-10326**
Difference between above two criterions	**25346**	**14006**	**--**
Percentage of PS points after refinement with respect to ASI method	**48.7%**	**71.0%**	**22.3%**

Majorly, the deformation is around three right canals originating from Prakasam dam. These three canals (Buckingham, Rivas and Bandaru canal) which pass through the city, are the major source of water for irrigation. In HH polarization, deformation ranges from +16 to -14 mm/year, whereas in VV it ranges from +12 to -19 mm/year. Positive values correspond to uplift, while negative values correspond to ground subsidence. Areas close to the river coast show movement away from the radar (subsidence), whereas areas far from the coast moved towards the radar (uplift). Figure 5 shows deformation pattern for HH and VV polarization around the three canals.

In both HH and VV, subsidence areas tend to deform continuously over time. By plotting time series deformation, we have observed an interesting pattern as shown in Figure 6. For subsidence points, we have observed a rise in displacement between September and November 2014 and a dip between October and December 2014. Remarkably, the shift between rise and dip (or vice versa) is observed in October. Even though mentioned pattern is observed at most of the points; there are few inconsistent points where this trend is not observed. It is also interesting to note that the pattern is irrespective of polarization.

Devastating HudHud cyclone hit the state of Andhra Pradesh in October 2014. The cyclone mostly affected Visakhapatnam, a well-known coastal city of Andhra Pradesh. Due to the cyclone, most of the coastal areas of the state experienced moderate to heavy rains before and after the event. There is a high chance of atmospheric effect on the 23-10-2014 RADARSAT-2 image due to the wide spread of clouds. The presence of atmosphere delays the C-band radar signal results in variation in phase and deformation estimates.

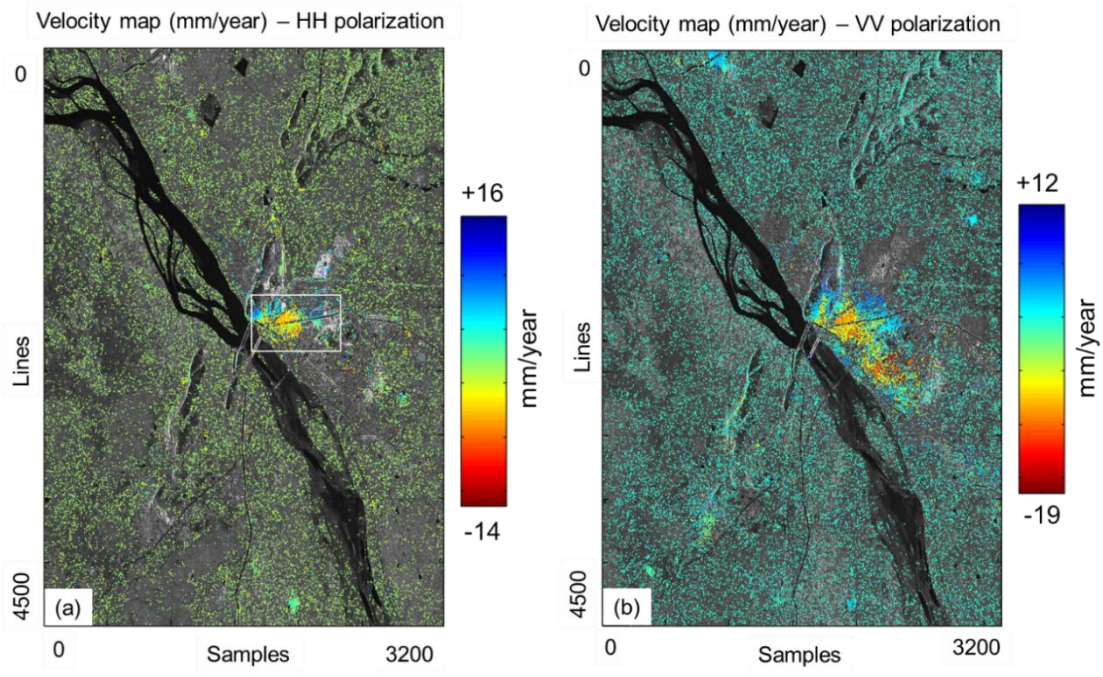

Figure 4: Velocity maps of HH and VV polarization over Vijayawada city. Clear deformation is observed in VV polarization due to its response to urban settlements. Maximum and minimum deformation rates are shown in mm/year. RADARSAT-2 Data and Products © MacDonald, Dettwiler and Associates Ltd. 2014 – All Rights Reserved. RADARSAT is an official trademark of the Canadian Space Agency.

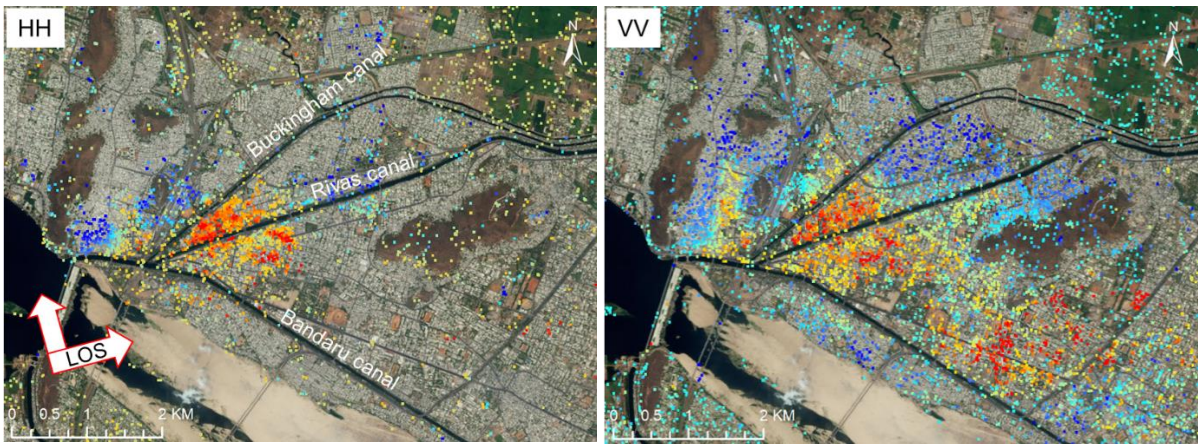

Figure 5: Deformation near the river coast and around three canals in HH and VV polarizations (the area is shown as a white rectangle in Figure 4). Moving far from the coast, VV shows uplifted areas, which are not observed in HH polarization. Colour scale is same as Figure 4. RADARSAT-2 Data and Products © MacDonald, Dettwiler and Associates Ltd. 2014 – All Rights Reserved. RADARSAT is an official trademark of the Canadian Space Agency.

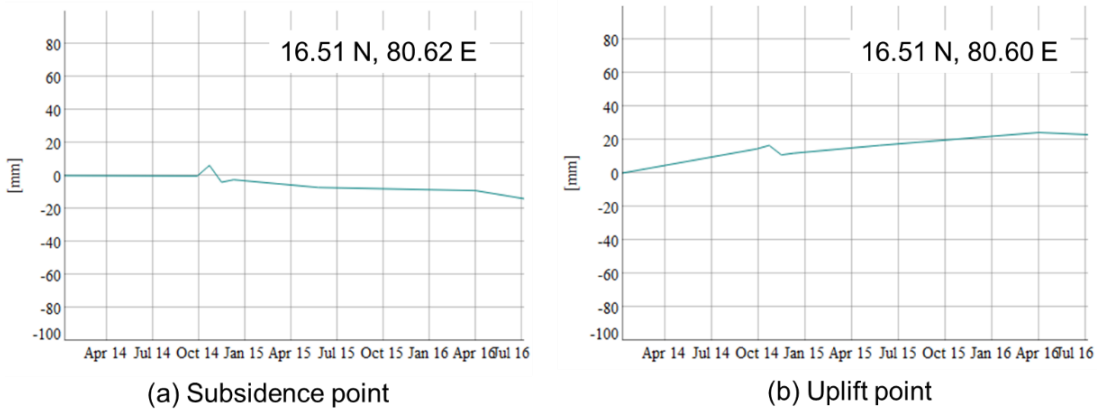

Figure 6: Plots showing deformation over time at the point 16.51N, 80.62E and 16.51N, 80.60E. Both plots show up and down pattern between October and December 2014.

5. CONCLUSION

RADARSAT-2 C-band Quad polarization data are analysed to study the effect of polarization on deformation estimates. Deformation results obtained using HH and VV polarization images are compared in terms of number of PS points and deformation estimates. Both polarizations show nearly similar deformation magnitude. Away from the river coast, due to its interaction with vertical oriented urban settlements, VV shows uplift areas that are not seen in HH polarization. Except between October and December 2014, observed deformation follows assumed linear deformation model. Presence of strong clouds delay the radar signal, which result in a swift in deformation estimate for all PS points. Our results portray that PS points and deformation identified using VV are better than HH polarization over a metropolitan area like Vijayawada. More detailed time series deformation can be studied using C-band Sentinel-1 Interferometric Wide Swath data with a low temporal gap (12 days). More images will lead to improvement in deformation measurements.

ACKNOWLEDGEMENTS

The authors thank MDA-GSI and Canadian Government for providing RADARSAT-2 data through project code SOAR-EI-5174. We are grateful to Mr. Kapil Malik and SARPROZ team for giving an evaluation copy of the software tool.

REFERENCES

Amelung, F., Galloway, D.L., Bell, J.W., Zebker, H.A., Laczniak, R.J., 1999. Sensing the ups and downs of Las Vegas: InSAR reveals structural control of land subsidence and aquifer-system deformation. Geology 27, 483–486.

Antonielli, B., Monserrat, O., Bonini, M., Cenni, N., Devanthéry, N., Righini, G., Sani, F., 2016. Persistent Scatterer Interferometry analysis of ground deformation in the Po Plain (Piacenza-Reggio Emilia sector, Northern Italy): seismo-tectonic implications. Geophys. J. Int. 206, 1440–1455.

Berardino, P., Fornaro, G., Lanari, R., Sansosti, E., 2002. A new algorithm for surface deformation monitoring based on small baseline differential SAR interferograms. IEEE Trans. Geosci. Remote Sens. 40, 2375–2383.

Colesanti, C., Ferretti, A., Novali, F., Prati, C., Rocca, F., 2003. SAR monitoring of progressive and seasonal ground deformation using the permanent scatterers technique. IEEE Trans. Geosci. Remote Sens. 41, 1685–1701.

Esmaeili, M., Motagh, M., 2015. PSInSAR Improvement using Amplitude Dispersion Index Optimization of Dual Polarimetry Data. Int. Arch. Photogramm. Remote Sens. Spat. Inf. Sci. 40, 175.

Ferretti, A., Prati, C., Rocca, F., 2001. Permanent scatterers in SAR interferometry. IEEE Trans. Geosci. Remote Sens. 39, 8–20.

Ferretti, A., Prati, C., Rocca, F., 2000. Nonlinear subsidence rate estimation using permanent scatterers in differential SAR interferometry. IEEE Trans. Geosci. Remote Sens. 38, 2202–2212.

Goldstein, R.M., Engelhardt, H., Kamb, B., Frolich, R.M., 1993. Satellite radar interferometry for monitoring ice sheet motion: application to an Antarctic ice stream. Sci.-N. Y. THEN Wash.- 262, 1525–1525.

Hanssen, R.F., 2001. Radar interferometry: data interpretation and error analysis. Springer Science & Business Media.

Hooper, A., 2008. A multi-temporal InSAR method incorporating both persistent scatterer and small baseline approaches. Geophys. Res. Lett. 35.

Hooper, A., Zebker, H., Segall, P., Kampes, B., 2004. A new method for measuring deformation on volcanoes and other natural terrains using InSAR persistent scatterers. Geophys. Res. Lett. 31.

Kampes, B.M., 2006. The stun algorithm. Radar Interferom. Persistent Scatt. Tech. 43–69.

Lanari, R., Mora, O., Manunta, M., Mallorquí, J.J., Berardino, P., Sansosti, E., 2004. A small-baseline approach for investigating deformations on full-resolution differential SAR interferograms. IEEE Trans. Geosci. Remote Sens. 42, 1377–1386.

Massonnet, D., Briole, P., Arnaud, A., 1995. Deflation of Mount Etna monitored by spaceborne radar interferometry. Nature 375, 567.

Massonnet, D., Holzer, T., Vadon, H., 1997. Land subsidence caused by the East Mesa geothermal field, California, observed using SAR interferometry. Geophys. Res. Lett. 24, 901–904.

Massonnet, D., Rossi, M., Carmona, C., Adragna, F., Peltzer, G., Feigl, K., Rabaute, T., 1993. The displacement field of the Landers earthquake mapped by radar interferometry. Nature 364, 138–142.

Ng, A.H.-M., Ge, L., Li, X., Abidin, H.Z., Andreas, H., Zhang, K., 2012a. Mapping land subsidence in Jakarta, Indonesia using persistent scatterer interferometry (PSI) technique with ALOS PALSAR. Int. J. Appl. Earth Obs. Geoinformation 18, 232–242.

Ng, A.H.-M., Ge, L., Li, X., Zhang, K., 2012b. Monitoring ground deformation in Beijing, China with persistent scatterer SAR interferometry. J. Geod. 86, 375–392.

Peltzer, G., Rosen, P., 1995. Surface displacement of the 17 May 1993 Eureka Valley, California, earthquake observed by SAR interferometry. Science 268, 1333.

Perissin, D., Wang, T., Wang, Z., 2011. The SARPROZ InSAR tool for urban subsidence/manmade structure stability monitoring in China https://www.researchgate.net/publication/228878770_The_SARPROZ_InSAR_tool_for_urban_subsidencemanmade_structure_stability_monitoring_in_China (accessed 9.14.17).

Rao, Y.S., Venkataraman, G., Rao, K.S., Snehmani, 2004. SAR interferometry for DEM generation and movemnet of Indian glaciers, in: IGARSS 2004. 2004 IEEE International Geoscience and Remote Sensing Symposium. Presented at the IGARSS 2004. 2004 IEEE International Geoscience and Remote Sensing Symposium, pp. 1128–1131. doi:10.1109/IGARSS.2004.1368612

Schmidt, D.A., Bürgmann, R., 2003. Time-dependent land uplift and subsidence in the Santa Clara valley, California, from a large interferometric synthetic aperture radar data set. J. Geophys. Res. Solid Earth 108.

Wegmuller, U., Walter, D., Spreckels, V., Werner, C.L., 2010. Nonuniform ground motion monitoring with TerraSAR-X persistent scatterer interferometry. IEEE Trans. Geosci. Remote Sens. 48, 895–904.

Werner, C., Wegmuller, U., Strozzi, T., Wiesmann, A., 2003. Interferometric point target analysis for deformation mapping, in: Geoscience and Remote Sensing Symposium, 2003. IGARSS'03. Proceedings. 2003 IEEE International. IEEE, pp. 4362–4364.